Precision Engineering 52 (2018) 183–191

Contents lists available at ScienceDirect

Precision Engineering

journal homepage: www.elsevier.com/locate/precision

A machine vision system for micro-milling tool condition monitoring

Yiquan Dai[a], Kunpeng Zhu[a,b,*]

[a] Institute of Advanced Manufacturing Technology, Hefei Institutes of Physical Science, Chinese Academy of Science, Huihong Building, Changwu Middle Road 801, Changzhou, 213164 Jiangsu, China
[b] School of Logistics Engineering, Wuhan University of Technology, Heping Road 1178#, Wuhan, 430063 Hubei, China

ARTICLE INFO

Keywords:
Tool wear
Tool condition monitoring
Machine vision
Micro milling
Digital image processing

ABSTRACT

Tool condition monitoring is a key issue in micromachining for part quality control because the excessive tool wear and abnormal tool conditions will significantly decrease the size accuracy of part and shorten the tool durability as well. In view of this, a novel configuration of machine vision system for online tool condition monitoring is presented to improve the part quality and extend the micro tool life. The vision system is committed to automated on-machine vision inspection for monitoring the progressive wear. This inspection system uses a telecentric lens with light source and a camera to minimize the errors in imaging. The control system drives a three dimensional motion platform carrying the imaging device to probe and grab in-focus image at the predetermined time interval of machining. In addition to the flank wear, three new wear variables are explored to enhance the robustness in prediction of tool wear state. Effective image processing algorithms are developed to reduce downtime. The effectiveness of the prototype system and the developed algorithms for tool wear extraction are verified by cutting experiments using two-flutter micro-milling tools, and the experimental results show that this novel on-machine vision inspection system is convenient and effective to measure the amount of progressive wear and reflect the trend of tool life.

1. Introduction

Micro-milling operations are extensively applied in producing miniature components with three-dimensional (3D) features especially for high precision parts of metallic alloys [1]. Tool condition monitoring (TCM) is very necessary to avoid tool's premature failure or extremely unpredictable tool life in a computer numerical control (CNC) machine [2], because the part quality is principally dependent on the cutting tool wear condition. The stable form of tool wear is flank wear which is empirically depicted as three stages including initial wear, steady state and severe wear. An accurate and reliable prediction of the start point in severe wear stage is always important in concerning. For example, Tansel et al. [3] propose to reduce the cutting feed rate according to the detected micro tool wear in order to decrease the surface damage and increase the micro tool life. On the other hand, if a tool breaks during the machining, surface damage is inevitable, which leads to wasted workpieces and less productivity. In micromachining, the micro tools may be broken in a few seconds under abnormal cutting condition or excessive worn state. The development of subsystem for tool wear inspection is an urgent demand and it is the main topic here.

The tiny shaft of a micro-milling tool is driven at extremely high rotational speeds with cutting materials in micro-scale. These features lead to critical issues in micro milling [4], such as size effects, relatively large vibrations, single-toothed cutting phenomena, and micro-burrs, which in turn cause uncertainty in measurement for feedback control [5]. Theoretically, the micro tool cutting-edge profile is an important factor that directly influences the final quality of a machined surface. The problem is that measuring the sharp edges of cutting tools is a very challenging work because it involves a small radius that requires high lateral resolution and high angles. It is also important to be able to measure a diverse range of heights at nanometres scale. Furthermore, the uncertainty in measurement will cause serious noise in micro-tool wear monitoring [6] which is very necessary to avoid excessive tool wear and maintain part tolerances [7]. The problem is that the existing methods or studies in the literature are mainly artificial inspecting or monitoring the indirect tool-state signals, which are seriously influenced by the noise in micro milling. In fact, most of investigators attempt to extract the indirect signals, such as forces [2] and AE (acoustic emission) [8], and then construct the relationship to the tool life, which is very difficult in practice considering the mentioned noise and contact disturbance. Martins et al. [9] adopt Neural Networks to identify the

* Corresponding Author at: Institute of Advanced Manufacturing Technology, Hefei Institutes of Physical Science, Chinese Academy of Science, Huihong Building, Changwu Middle Road 801, Changzhou, Jiangsu, 213164, China.
E-mail address: zhukp@iamt.ac.cn (K. Zhu).

https://doi.org/10.1016/j.precisioneng.2017.12.006
Received 15 May 2017; Received in revised form 4 December 2017; Accepted 5 December 2017
Available online 07 December 2017

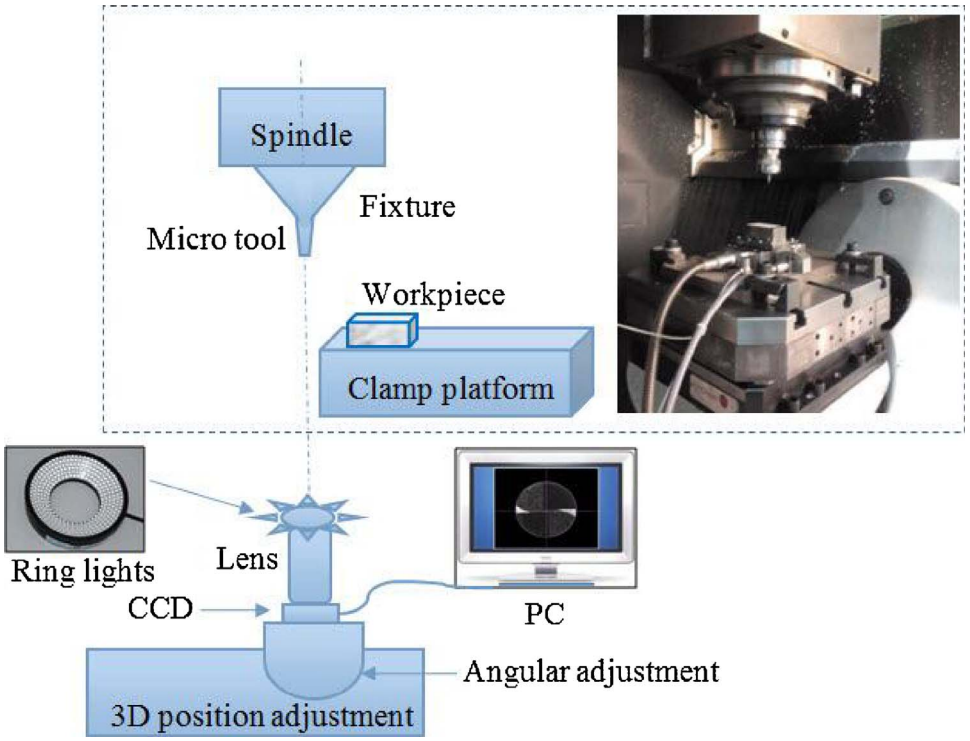

Fig. 1. Experimental setup.

meaningful information from the disturbing and fuzzy variables; Wang et al. [10] present the probabilistic kernel factor analysis (PKFA) as a novel intelligence algorithm to analysize multisensory measurements of machinery conditions. On the other hand, the paper adopts machine vision to measure the amount of tool wear directly, and for the first time the vision inspection subsystem is integrated within the CNC system to realize automatic cooperation in machining.

Though various direct and indirect tool wear monitoring techniques have been developed [11], there is still no consensus with the best choice for micro milling tool wear monitoring especially considering the lack of automation and robustness. Comparatively, Signal-to-Noise in micromachining will decrease in an indirect method because of the size effects and relatively large vibrations [12], and the machine vision as a direct method has many attractive advantages [13]. Especially, the vision method can avoid contact disturbance from measuring setups to the tiny tools and can directly measure the progressive tool wear for analysis. In a machine vision system, digital image processing algorithms and light source arrangement are very important factors for high precision tool wear inspection. At the same time, noise in imaging, defocussing, camera vibration, incline from shooting surface, speckles in image due to micro metal particles, and stray lights reflected by object surfaces should also be considered with countermeasures. In view of these issues, Ratnam et al. [14] attempt different image edge detection and line fitting methods in focus of nose radius wear measurement. Szydłowski et al. [15] design an image fusion system based on wavelet transform to resist defocussing in imaging of micro milling tools. Wang et al. [16] investigate the factors that influence the image segmentation so as to extract the wear region accurately. Pfeifer et al. [17] and Yamashina et al. [18] mainly devote to light source arrangement and suggested to capture images with special angles of incidence of the illuminating light to enhance the image edge of wear region. Lim et al. [19] supply a theoretical analysis of edge diffraction in imaging to guide the light source arrangement. Duan et al. [20] introduce the famous Geometric Active Contour model for image segmentations to resist the noise. The problems of lens distortion and defocussing are also considered by Fan et al. [21].

These contributions together with other works reviewed in [13,22] have made lots of achievements. Considering the features above, convenient and effective tool condition monitoring systems especially for micro milling tools are still need to perfect or develop. Moreover, even the variables such as flank wear and crater wear, suggested in ANSI/ASME B94.55M-1985 standard for the extents of conventional tool wear indication are insufficient [23,24]. To the date, whether such variables are suitable for micromachining cases is still not ascertained in the literature, and there is no such standard for micromachining at all. Accordingly, multivariate is a good idea to enhance the robustness of tool life indication [24], such as the work by Dutta et al. [25] that take advantage of flank wear of tools and machined surface textures in analysis.

In view of the issues mentioned above, this paper proposes a machine vision system especially for micro milling tools. The time intervals are identified or added in CNC program codes for the progressive wear inspection. To overcome the difficulties in on-line micro imaging of tool cutters, the vision inspection module runs automatically by program control of motors carrying the imaging device. The novel algorithms are also designed considering the characteristics of the images to extract the wear robustly. In experimental verifications, the developed prototype can run automatically in conjunction within a micro milling center using two-flutter micro-milling tools. Moreover, several variables indicating the wear state are explored to enhance its robustness.

2. Tool wear inspection system

2.1. Experimental setup

The total system is illustrated in Fig. 1, and the vision inspection module is mainly arranged below the original CNC structures. The kernel framework of a precision milling center remains unchanged, as schematically depicted inside the dashed rectangle in Fig. 1. Specifically, the tool images are captured in process with an Olympus CCD (charge-coupled device) with tele-centric micro lens after cleaning, which has more than 200 times enlargement. These raw images are then processed with the developed image processing system written in

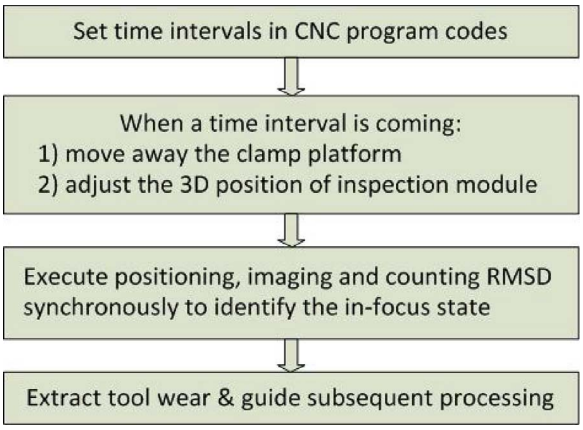

Fig. 2. Procedures of tool wear monitoring.

C++ program. The angular adjustment is a tripod ball-head stand commonly used in videography; the 3D position adjustment is assembled with three linear motors and the z-direction (up & down) is controlled with a higher resolution of 0.65 mm per pulse by C++ program codes. The working flow of the system is illustrated in the chart Fig. 2.

2.2. Procedures

As presented in the working flow chart Fig. 2, the vision inspection module cooperates with the existing micro-milling center by inserting CNC program codes to realize an automatic tool wear monitoring. At the first step, time intervals are identified or added in CNC program codes to wake up tool wear inspections during processing. For the purpose of insurance, one minute is an enough length of time interval for verification in the prototype system and it can be shorten further by estimating the necessary motor pulses in position adjustment. In experimental verification later, the sustained machining time is 100 s, which means that after every 100 s of machining, the tool wear will be inspected once in 60 s until obvious damage or condition variation.

When a time interval is coming during machining in the second step, drive the clamp platform together with workpiece to make enough room for tool wear inspection. In practice, the actions of position adjustment can be achieved by controlling the number of motor pulses in program codes. The number of pulses corresponding to the lens in-focus position can be calibrated before machining and minor adjustment to the in-focus position in inspection is carried out by algorithm presented later. For example, a linear reciprocating motion can be accomplished by driving a number of positive or negative pulses within the linear motor driving codes. The rest steps are mainly based on image processing, which will be presented later.

2.3. Tool wear characterization

The resolution of the image is 1024 × 768 with 8 bits per pixel as shown in Fig. 5 without pre-processing. The diameter along major axis of the two-flutter micro-milling tool (C-CHES 2008-0180) is 800 mm by tool manufacturer and the diameter along minor axis is 660 mm by measurement. In this manner of light source arrangement in Fig. 1, the worn regions at the end of the tool are illuminated perpendicularly to avoid diffraction distortion at the edges, such as the concerning in [18,19]. At the same time, the minor cutting edges will directly reflect the incident light and cause brightness because of the shiny cutter edges from friction. Due to this surface characteristic, the intensity of the reflected light from the contacting surface is much higher than that from the unworn tool surface or from the background. In fact, the two white regions in the image can be used as good indictors of tool life, and algorithms will be developed to establish the relationship between the variables of the white regions and tool life history.

The amount of tool wear will be extracted quickly with the designed algorithm depicted in next section to guide subsequent machining. As verification, several images are also shown in Fig. 3 for a visual representation of this relationship. As seen in Fig. 3, both the symmetric white regions corresponding to minor cutter edges are increasing with the extension of time. Therefore, variables for characterization of the incremental worn areas manifested with white pixels will be identified to explore the potential in revealing tool life.

Castejón et al. [24] are aware of the importance of finding out the best description of the wear regions in image, and then nine geometric descriptors are introduced. However, their descriptors are calculated from basic variables in inspection, and the measuring accuracy of each variable is not fully considered. In the situation here, there are four variables, area of wear land (S_1 and S_2), flank wear (VB_1 and VB_2), radial wear (RW_1 and RW_2), and diameter wear (DW_1 and DW_2) which are available to indicate the extent of wear as shown in Fig. 4. In practice, the flank wear is widely accepted for tool life indication in the literature, and the area of wear land can be simply extracted without considering the rotation angle at imaging time. In addition, both the radial wear and diameter wear are useful indicators for tool life prediction [26], which are all verified in experiments later.

3. Tool wear inspection method

3.1. Image acquisition

A novel mechanism is developed to identify and grab the in-focus image by real-time counting root mean square deviation (RMSD) in the general Region of Interesting (ROI). The algorithm for ROI recognition is specified in 3.2.4 section. In the developed program, the three threads of motor driving, image grabbing and RMSD counting are executed synchronously. The in-focus state is corresponding to the maximum of RMSD.

$$RMSD = \sqrt{\frac{1}{n}\sum_{i=1}^{n}(f_i - \overline{f})^2} \tag{1}$$

where f denotes grey value of digital image; $\overline{f}$ describes the averaging operation; n stands for the number of pixels in ROI. As shown in Fig. 5, the ROI is identified as the pixels inside rectangle.

The in-focus state can be identified and kept as a number of pules opposite to initial state in advance. With the tool wear increasing, the in-focus state can be adjusted by moving up and down, meanwhile real-time counting RMSD of ROI in digital images. That is to say, position adjustment, grabbing image and counting RMSD are executed

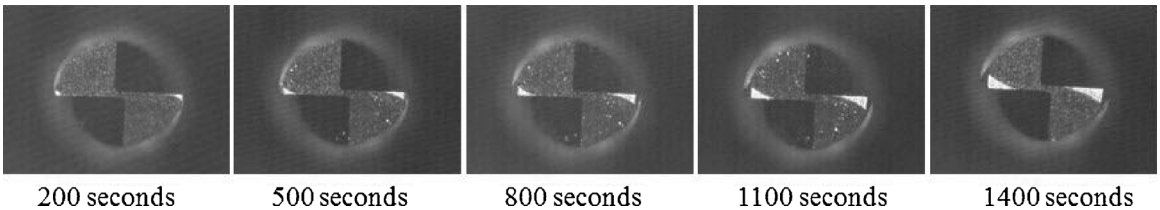

Fig. 3. Representative images along tool life history.

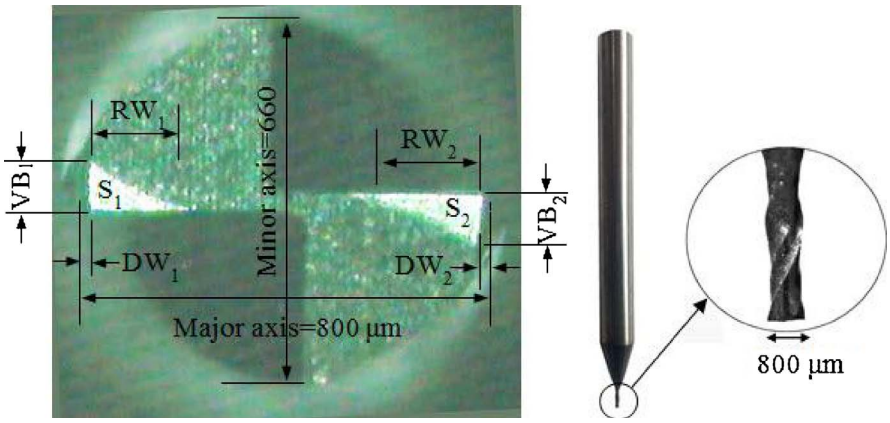

Fig. 4. Variables defined for micro milling tool wear indication.

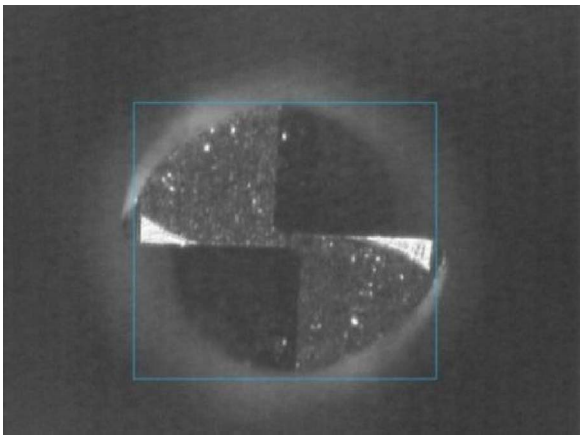

Fig. 5. Image in real time acquisition state.

synchronously to save time, and the in-focus image is recognized according to the maximum RMSD without suspending the motors.

3.2. Tool wear measurement

The developed algorithm includes steps listed in Fig. 6 for an overview and the main idea of each step is explained. There are mainly

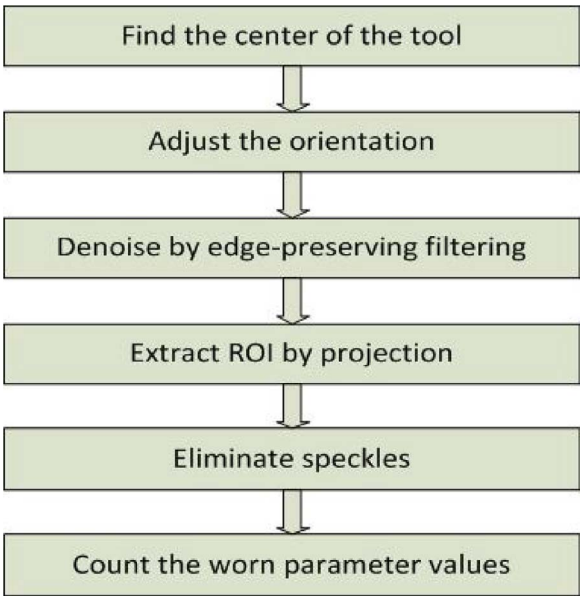

Fig. 6. Schematic of the image processing algorithm.

two motivations in the total algorithm. The first is to correct the angle by rotation image so that the flank wear can be identified conveniently (flank wear are corrected to be vertical). The next is to suppress noises and detect wear variables accurately. Several subroutines are developed especially considering the characteristics of the tool wear images. In addition, the processing speed is also very important because the effective tool life is even less than twenty minutes.

3.2.1. Identification of the tool center

The tool in the grabbed image is different angle and position. In order to extract the wear variables conveniently, adjusting the angle of the image is a good choice so that the wear can be counted in horizontal or vertical direction. Thus, the exponential transform of an image is introduced for image enhancement to find the center of the tool in image. As seen in Fig. 5, the worn regions are distinguished from other regions with larger grey values. As a result, this distinguishes can be further enhanced by the exponential transform:

$$g_i = f_i^m \tag{2}$$

where f denotes the grey value of a given pixel i, m stands for the power index. After this exponent operation pixel by pixel, the total image will be re-scaled for showing by:

$$f_i = \frac{255}{g_{max} - g_{min}}(g_i - g_{min}) \tag{3}$$

where the subscripts (max and min) describe the statistical operations upon all pixels.

In order to show the effects of this step by formulas 2 and 3, the results from different power index are shown in Fig. 7. The white regions are highlighted with increasing of the power index m. Subsequently, only the two largest white regions are preserved. Thus, it is possible to find out the two centers by counting the center of grey gravity in four quadrants. The center of grey gravity can be calculated by:

$$\begin{cases} x_c = \dfrac{\sum_{i=1}^{w}\sum_{j=1}^{h} x_i g_{ij}}{\sum_{i=1}^{w}\sum_{j=1}^{h} g_{ij}} \\ y_c = \dfrac{\sum_{i=1}^{w}\sum_{j=1}^{h} y_i g_{ij}}{\sum_{i=1}^{w}\sum_{j=1}^{h} g_{ij}} \\ g_{ij} = \begin{cases} 0, f_{ij} < T \\ 1, f_{ij} \geq T \end{cases} \end{cases} \tag{4}$$

where w and h stand for the width and height of the image respectively, the threshold value T can be 200 in practice and it is not critical in magnitude after exponential transform as seen in Fig. 7.

3.2.2. Adjusting the orientation

The center of grey gravity operations can be carried out within the

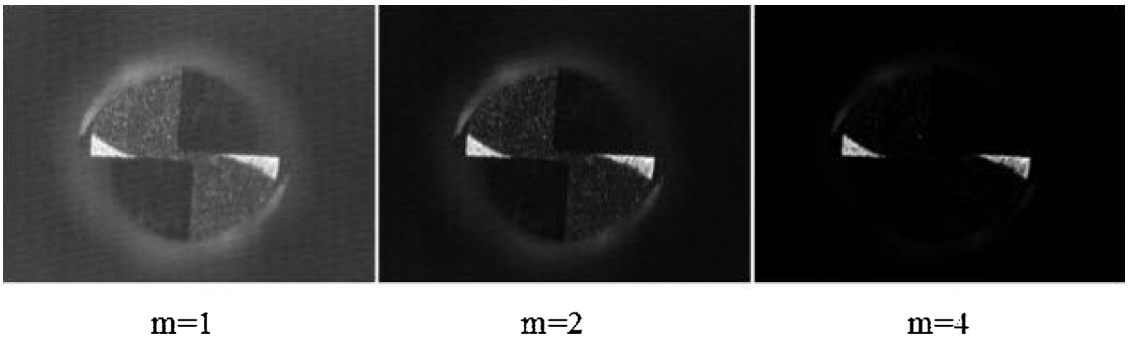

Fig. 7. Effects of exponential transform.

total image to obtain the total center and then carried out within four quadrants partitioned by total center respectively. In this way, the two center positions are obtained and used to ascertain the angle A:

$$A = \arctan\frac{y_{c1} - y_{c2}}{x_{c1} - x_{c2}} \tag{5}$$

As mentioned, the single-toothed cutting is difficult to avoid and through trying in experiments, the extents of wear in the two flutters are still not the same. Therefore, the two white worn regions are not of the same size and the angle corrections by rotating the images can only support accuracy within 5°. However, these results can be achieved quickly by the algorithm.

3.2.3. Denoising by edge preserving filtering

By now, there is no resistance to noise considered in the scheme of exponential transform and angle correction. Considering the speckles in image due to micro metal particles and noise in imaging, an edge-preserving filter is necessary to suppress the noise in image. There are several famous filters available for edge-preserving smoothing, including infinite symmetric exponential filter (ISEF) [27], bilateral filter [28], guided filter [29], and other intelligent filters [30]. Comparatively, the ISEF filter is more suitable for the application considering that the others are not linear translation invariant (linear output) [30]. Moreover, the exponential function in ISEF is super than the widely used Gaussian function bilateral filters in approximation the steep boundaries in image here [27]. Moreover, updating filter coefficients pixel by pixel results in the low arithmetic speed in bilateral filtering. While the guided filter is also slowed greatly in finding local direction before filtering, and intelligent filters may lead to an unsteady output or variables which should be prepared carefully. The improved two-dimensional ISEF filter is given by

$$\begin{cases} f(\mathrm{r}) = \frac{-\ln(b)}{2} b^{r} \\ r = \sqrt{x^2 + y^2} \\ c(x, y) = \frac{f(r)}{\sum f(r)},\ r \le R \end{cases} \tag{6}$$

where x and y are coordinates with origin locating at the center of filter window, b is the smoothing coefficient which is assigned 0.95 in practice, the filter coefficients $c(x, y)$ are normalized within truncation radius R which is assigned 15 in discretization for acceleration. Inevitably, smoothing will corrode the edges with clear boundary. The designed scheme below is powerful to remedy this insufficient.

$$g_i = Max\{f_{ISEF}, f_i\} \tag{7}$$

where f_{ISEF} stand for the result from ISEF filtering of pixel i, f_i is the original grey value of pixel i.

3.2.4. Extracting the ROI by projection

In order to fast calibrate the scale from pixel to micron and correct the angle accurately in ROI extraction, the projection algorithm is designed. The presented projection operation is to count the lightness in each row or col following re-scaling for exhibition. The two steps in projection in x and y directions can be expressed as:

$$\begin{cases} Px(j) = \sum_{i=1}^{w} f(i, j), j \in [1, h] \\ Py(i) = \sum_{j=1}^{h} f(i, j),\ i \in [1, w] \end{cases} \tag{8a}$$

$$\begin{cases} PX(j) = \frac{w}{Px_{max} - Px_{min}}(Px(j) - Px_{min}), j \in [1, h] \\ PY(i) = \frac{h}{Py_{max} - Py_{min}}(Py(i) - Py_{min}),\ i \in [1, w] \end{cases} \tag{8b}$$

where $f(i, j)$ denote the grey value at pixel (i, j), subscripts of max and min stand for the highest and the lowest values, w and h are the width and height of the image respectively.

As seen in Fig. 8, image (a) is an original image in which the major axis has a more or less 4° deviation to horizontality in the result of second step. After ISEF filtering, the projected results in (b) and (c) are from rows (projection in x direction) and cols (projection in y direction) respectively, and scaled within the same size of the image for better exhibition. The image (d) is a combination of (a), (b), and (c) to reveal the relative positions of significant points in projection, as marked in small circles.

In this way, the ROI is enclosed by significant points as the four squares formed by dashed lines in Fig. 8(a). The cutter edges are wearing out but the cutter backs are not changed. Therefore, the high-precision angle for correction can be obtained by rotating a given degree of angle and probing the lowest of the center significant point in Fig. 8(c). The scale between pixel and micron can be extracted from the distance between off-center significant points in Fig. 8(b). This scale is calibrated as 660/478 ≈ 1.38 mm/pixel and experiments show that its fluctuation among images is negligible. The result of angle correction is shown in Fig. 9(a) together with the scale values. The circle is drawn according to the extracted diameter of minor axis. Then, by edge detection at flanks along the major axis (horizontal), the length of major axis can be obtained according to the scale as shown in Fig. 9(b). In this way, the diameter wear (DW_1 + DW_2) can also be calculated (800 − 732 = 68 mm).

3.2.5. Eliminating speckles

After angle correction and edge preserving filtering, a threshold value of 200 is possible to extract the wear regions. As a comparison, results from mean filter and the designed edge preserving filter both using the same filter window size of 15 are exhibited in Fig. 10. The regions from image binarization have been enlarged and located at the side of their original positions in the cutter images. The boundary lines of their white areas have been integrated with positional correspondence in the original cutter images. The worn areas manifested by white pixels are extracted insufficiently by mean filtering and binarization in Fig. 10(a).

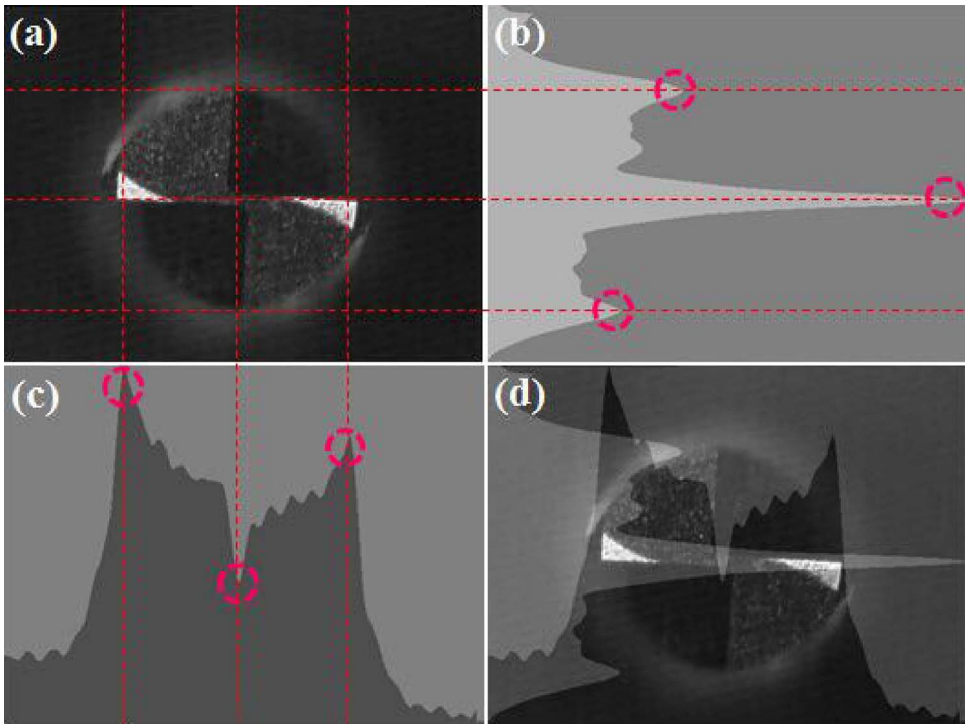

Fig. 8. Projection for ROI.

However, the presented edge preserving filtering can give a very accurate result in Fig. 10(b), which shows that the mechanism of formula (7) is powerful to correct the distortions due to smoothing. Subsequently, the white speckles can be eliminated by comparing the size of the regions. The two largest white areas indicate worn regions and others can be eliminated. After operations mentioned above, these variables can be obtained directly by counting the number of pixels in dimensions.

4. Experimental verification

4.1. The experiment

A total of 12 experiments were conducted to validate the designed tool wear monitoring system at different working conditions (Table 1). The machine used in the experiments was a five-axis MAKINO V55 vertical milling center driven by a 22kw spindle drive motor. The micro tools used in this study were 800 mm diameter micromilling tools with the helix and shank taper angles 30 and 16°, respectively. They are Tungsten Carbide tools, with Titanium Aluminum Nitride coatings. The workpiece materials used were pure copper and steel T4. Tool wear image was originally captured and measured using the Olympus Toolmakers microscope (213 times enlargement). More experimental setup can also be found in [31].

4.2. Experimental results and discussion

A group of results are shown in Fig. 11. The selected variables show steady trends with the time increment and can reveal the extent of wear in varying degrees. On the other hand, there is still no consensus in the literature with which is the best variable for micro tool wear indication. In fact, many investigators attempted different descriptors [23,24,32,33,], and accuate measurement is undoubtedly a prerequisite. There is an agreement on the necessity of avoiding single-toothed cutting phenomena in micromachining [34,35], however, it is very difficult to avoid in action and the differences of worn amplitude with two flutters (VB1 and VB2) are obvious as shown in Fig. 11. The two flutters are the same in imaging because of symmetry, which may lead to wrong correspondence between wear value and flutter. Therefore, the results are all extracted discriminatively by comparing the wear size at each step. A reference point supports this rule too.

Comparatively, the trends from flank wear Fig. 11(a) and areas of wear land Fig. 11(b) agree with the theoretical prediction [11] and the results of flank area wear predicted in [36]. It is observed that the more severe tool wear corresponding to greater wear area as shown in Fig. 3. The quantitative statistics of the areas of wear lands in Fig. 11(b) are

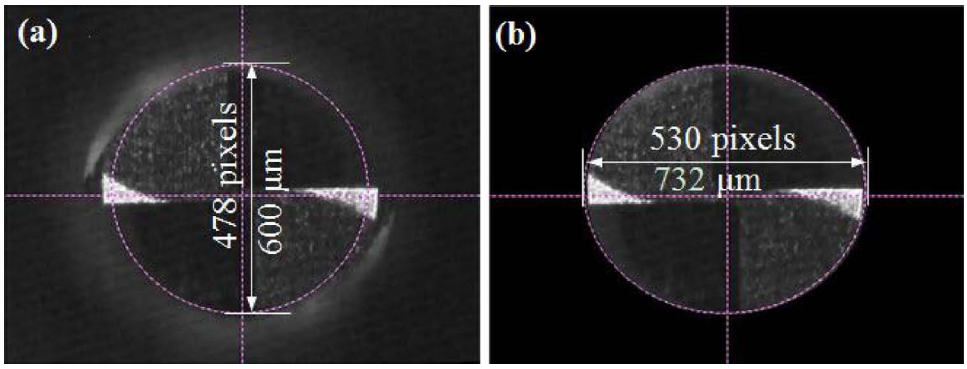

Fig. 9. Extracted ROI.

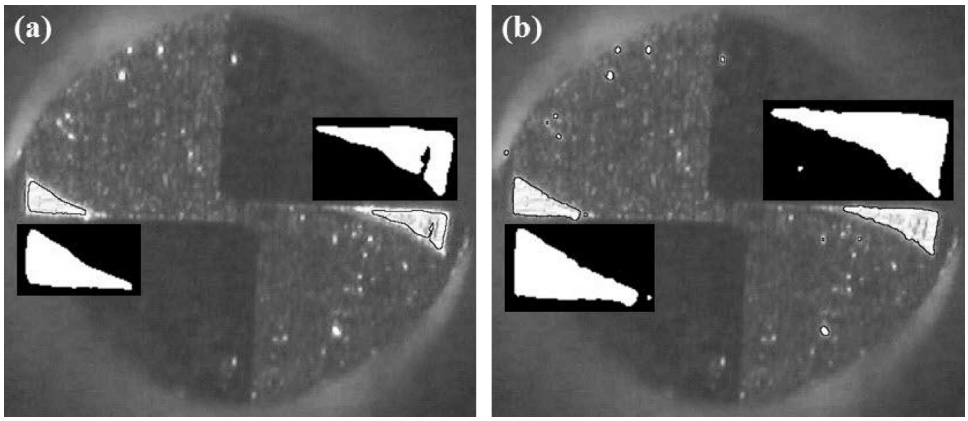

Fig. 10. Results of image binarization after mean filtering and the proposed method.

Table 1
The experimental working conditions.

Test	Spindle speed N (rpm)	Axial depth of cut ap (mm)	Radial engagement ae (mm)	Feed rate V_f(mm/min)
1	12,000	0.060	0.100	0.120
2	12,000	0.080	0.100	0.120
3	12,000	0.100	0.150	0.120
4	18,000	0.100	0.150	0.150
5	18,000	0.120	0.175	0.150
6	18,000	0.100	0.175	0.150
7	24,000	0.100	0.200	0.180
8	24,000	0.120	0.200	0.180
9	24,000	0.150	0.250	0.180
10	30,000	0.120	0.250	0.150
11	30,000	0.150	0.300	0.150
12	30,000	0.120	0.300	0.150

also show a steady trends that will benefit wear prediction even better than flank wear considering the value amplitude and stable tendency. Because of the friction and ploughing effect between the cutting tool and workpiece, there are micro burs due to adhered chips on the tool ends, as randomly and sparsely distributed speckles shown in Fig. 10, which are imaged as noises or connecting to the white wear lands. This is the main reason for the unsteady fluctuation on the tool wear curves in Fig. 11. In order to improve it, an air cock is aimed to blow away the burs, however, the effect is limited. On the other hand, it is also necessary to clean the tool end before inspection in traditional off-line measurement by tool microscope. Considering the cleaning may cause new damages and time consuming for the micro tools, multivariable monitoring is a good choice. For the severe wear stage, there is a jump of wear rate at about 1400 s, which is considered to be corresponding to the start of severe wear stage. The fluctuations from the two flutters result from the single-toothed cutting phenomena and noise from burrs on the cutter [37] as shown in Fig. 10.

There is no report concerning the diameter wear as shown in Fig. 12(a), and only the total wear is given due to accuracy of measurement (the amounts of wear at the two flutters are different and thus it is difficult to ascertain them respectively before identifying the center position). The fluctuation after 1200 s is about 1 pixel. However, the curve also gives light to revealing the tool life from the early trend, especially the point of inflection at about 1300 s close to the time of wear rate jump in Fig. 11(a). By artificial measurement carefully, it is also found that the diameter wear is indeed to be steady when the time is close to the tool's life. The Radial wear isalso supplied in Fig. 12(b) though they are sensitive to the sharp corner of the delta-shaped white regions. Experiments show that the curvilinear trends reflect the progressive worn extent. At the same time, there is also no report concerning the difference between the two flutters and the experimental results indicate that the wear from the two flutters tend to be equal in the end of steady state. Tool run-out is believed to be one of most important reasons for this asymmetric cutting [38]. Tool run-out plays an important role in micro milling because the ratio between tool run-out and feed per tooth is very high, which seriously influences the instantaneous undeformed chip thickness. In some cases, tool run-out is so high that just one flute cuts the material, generating an asymmetric cutting [38]. Castro [39] adopted a laser interferometer to measure the spindle rotation errors of machine tools with accuracy high enough. However, the special sphere affixed at the end of a wobble device which is clamped in the spindle will influence the normal movement due to associated mass, and the influence will be more obvious for micro tools. In our experiments, the cutter's coating thickness is reducing with machining and it is gradually becoming blunt, thus the further wear rate is relatively slowing. Furthermore, the differences of worn amplitude from the two flutters can also be explained as the differences of flutter cutters' contact area with the workpieces specially appearing in micromachining, as revealed by Li et al. [40].

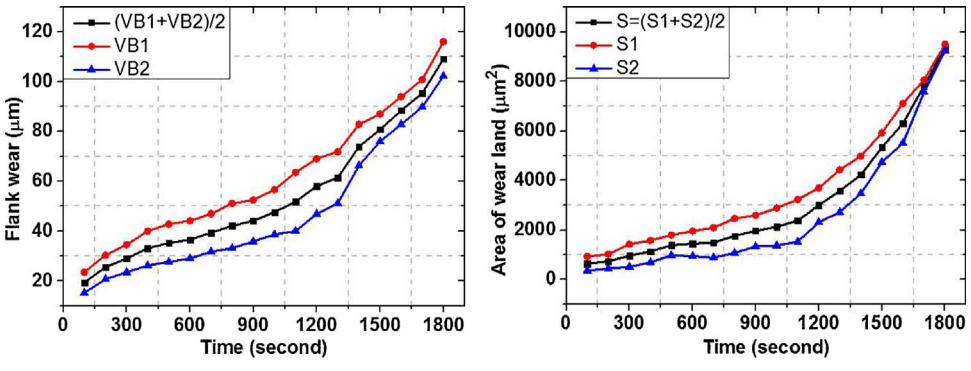

(a) Flank wear (b) Area of wear land

Fig. 11. Flank wear extracted by mean filtering.

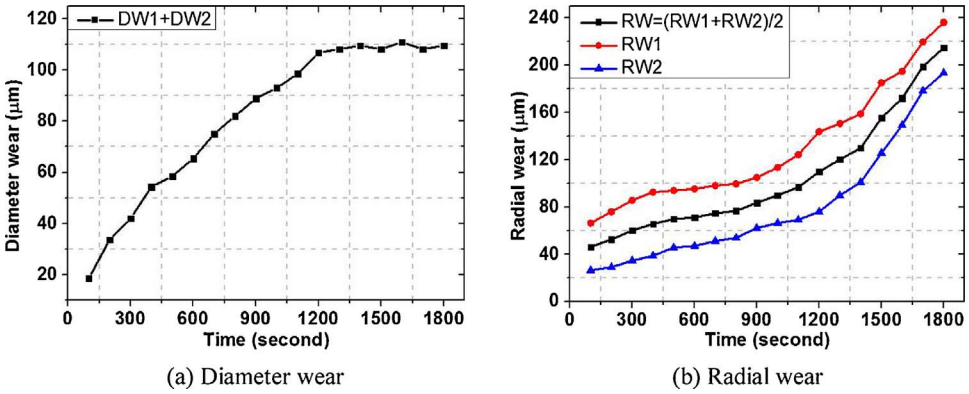

(a) Diameter wear (b) Radial wear

Fig. 12. Results of diameter wear and radial wear.

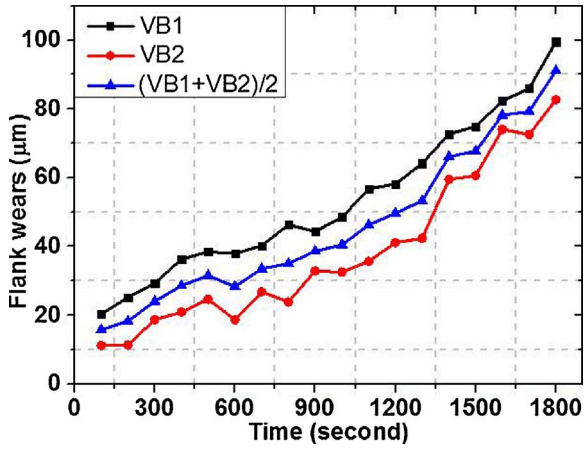

Fig. 13. Flank wear extracted by mean filtering.

Overall, the trend of wear area is steadier and is possible to evaluate the life of micro tools, such as estimating the average tool life or worn stages roughly. In fact, it has integrated more factors to indicate the tool state, and the formats of flank wear, radial wear and diameter wear are partly synthesized in it. At the same time, the flank wear, radial wear and diameter wear are also meaningful to monitor and identify the abnormal conditions by identify the jump of worn rate. Considering the small scale in micromachining, there are still a lot of unclear factors that have been simply considered as noises in the literature. Such noises may cause sudden abnormality such as tool breakage and tipping which are detrimental to the workpieces and even damage the part. Both steady trend prediction and abnormality identification are necessary. The further step is to improve machining operations, then to extend the tool life after monitoring the wear by the inspection system. The method proposed by Tansel et al. [3] is a good strategy, and it reduces the cutting feed rate when abnormality is identified or the evaluated worn stage is coming. The method does save the tool life in experiments as verified by Tansel. However, a quantitative assessment of efficiency and cost is difficult to carry out at present, and more instances in actual machining are necessary to collect statistical data in the future.

4.3. Accuracy analysis

In experiments, there are mainly three factors influences the repeatability of measurement. The first one is the stationary motion of the motor in imaging. Lowering motor's speed during focusing is possible to improve the quality of image to some extent. At the same time, the incline between the lens and the tool end should be avoided by system test running before processing. The second factor is denoising algorithm that is also concerned in many machine vision based TCMs. In contrast, the proposed edge preserving filtering supports a more accurate wear extraction than mean filtering, as seen in Fig. 10. The flank wear extracted by mean filtering are also shown in Fig. 13. Comparing with Fig. 11 (a) and Fig. 13, the overall amplitude from mean filtering is reduced, as illustrated in Fig. 10. At the same time, the range of the curve fluctuates more greatly due to false boundary recognition as shown in Fig. 10 (a). In addition to filtering, the influence from threshold value is insignificant to disturb the curves' total trends.

The last main factor concerning the repeatability of measurement is the micro burrs adhered to the boundary of the cutters. This is part of the reason for the curves trend fluctuation in Figs. 11 and 12. As a result, the precision is about 1.38 mm as calibrated in section 3.2.4 without unforeseen circumstances.

5. Conclusions

Premature failure is a major problem in micromachining. In order to successfully predict the micro tool life, the paper develops an automated machine vision system for tool condition monitoring. The image processing algorithms are developed according to the characteristics of micro milling to extract the progressive tool wear. In addition to the flank wear, new variables are proposed to reflect the tool wear state. Experiments have shown that area of wear land is suitable to forecast the tool wear stages and other variables are possible to identify the abnormality in cutting. The strategy in utilization the inspection system is to reduce the cutting feed rate when abnormality is identified or the evaluated worn stage is coming. There is no sudden failure happened with the sample tools and the proposed algorithms support the developed system in these verification experiments. In the future, the more appropriate feed rate is possible to be studied in depth with the detected tool condition and further explore the potentiality of micro tools.r

Acknowledgement

This project is supported by National Natural Science Foundation of China (Grant No.51475443), and the CAS 100 Talents Program, Chinese Academy of Sciences. The authors would like to thank the National University of Singapore for the permission of using these data for the research.

References

[1] Chae J, Park SS, Freiheit T. Investigation of micro-cutting operations. Int J Mach Tools Manuf 2006;46:313–32.
[2] Patra K, Jha AK, Szalay T, Ranjan J, Monostori L. Artificial neural network based tool condition monitoring in micro mechanical peck drilling using thrust force signals. Precis Eng 2017;48:279–91.
[3] Tansel I, Nedbouyan A, Trujillo M, Tansel B. Micro-end-milling—II. Extending tool life with a smart workpiece holder (SWH). Int J Mach Tools Manuf 1998;38:1437–48.
[4] Aramcharoen A, Mativenga PT. Size effect and tool geometry in micromilling of tool steel. Precis Eng 2009;33:402–7.

[5] Sun YX, Xiong ZH. An optimal weighted wavelet packet entropy method with application to real-time chatter detection. IEEE/ASME Trans Mechatron 2016;21:2004–14.
[6] Tansel IN, Arkan TT, Bao WY, Mahendrakar N, Shisler B, McCool D. Tool wear estimation in micro-machining. Part I: tool usage?cutting force relationship. Int J Mach Tools Manuf 2000;40:599–608.
[7] Lee HC, Chang YC, Huang YS. A reliable wireless sensor system for monitoring mechanical wear-out of parts. IEEE Trans Instrum Meas 2014;63:2488–97.
[8] Zhang C, Brinksmeier E, Rentsch R. Micro-USAL technique for the manufacture of high quality microstructures in brittle materials. Precis Eng 2006;30:362–72.
[9] Martins CHR, Aguiar PR, Frech A. Tool condition monitoring of single-point dresser using acoustic emission and neural networks models. IEEE Trans Instrum Meas 2014;63:667–79.
[10] Wang JJ, Xie JY, Zhao R. A new probabilistic kernel factor analysis for multisensory data fusion: application to tool condition monitoring. IEEE Trans Instrum Meas 2016;65:2527–37.
[11] Dimla DE. Sensor signals for tool-wear monitoring in metal cutting operations—a review of methods. Int J Mach Tools Manuf 2000;40:1073–98.
[12] Tansel I, Trujillo M, Nedbouyan A, Velez C, Bao WY. Micro-end-milling—III. Wear estimation and tool breakage detection using acoustic emission signals. Int J Mach Tools Manuf 1998;38:1449–66.
[13] Dutta S, Pal SK, Mukhopadhyay S, Sen R. Application of digital image processing in tool condition monitoring: a review. CIRP J Manuf Sci Technol 2013;6:212–32.
[14] Shahabi HH, Ratnam MM. In-cycle monitoring of tool nose wear and surface roughness of turned parts using machine vision. Int J Adv Manuf Technol 2009;40:1148–57.
[15] Szydłowski M, Powałkaa B, Matuszakb M, Kochmańskia P. Machine vision micro-milling tool wear inspection by image reconstruction and light reflectance. Precis Eng 2016;44:236–44.
[16] Wang WH, Hong GS, Wong YS. Flank wear measurement by a threshold independent method with sub-pixel accuracy. Int J Mach Tools Manuf 2006;46:199–207.
[17] Pfeifer T, Wiegers L. Reliable tool wear monitoring by optimized image and illumination control in machine vision. Measurement 2000;28:209–18.
[18] Yamashina H, Okumura S. A machine vision system for measuring wear and chipping of drilling tools. J Intel Manuf 1996;7:319–27.
[19] Lim HS, Son SM, Wong YS, Rahman M. Development and evaluation of an on-machine optical measurement device. Int J Mach Tools Manuf 2007;47:1556–62.
[20] Duan GF, Chen YW, Sukegawa T. Automatic optical flank wear measurement of microdrills using level set for cutting plane segmentation. Mach Vision Appl 2010;21:667–76.
[21] Fan KC, Lee MZ, Mou JI. On-line non-contact system for grinding wheel wear measurement. Int J Adv Manuf Technol 2002;19:14–22.
[22] Kurada S, Bradley C. A review of machine vision sensors for tool condition monitoring. Comput Ind 1997;34:55–72.
[23] Astakhov VP. The assessment of cutting tool wear. Int J Mach Tools Manuf 2004;44:637–47.
[24] Castejón M, Alegre E, Barreiro J, Hernández LK. On-line tool wear monitoring using geometric descriptors from digital images. Int J Mach Tools Manuf 2007;47:1847–53.
[25] Dutta S, Kanwat A, Pal SK, Sen R. Correlation study of tool flank wear with machined surface texture in end milling. Measurement 2013;46:4249–60.
[26] Jackson MJ, Robinson M, Hyde LJ, Rhodes R. Neural image processing of the wear of cutting tools coated with thin films. J Mater Eng Perform 2006;15:223–9.
[27] Shen J, Castan S. An optimal linear operator for step edge detection. CVGIP. Graphical Models Image Process 1992;54:112–33.
[28] Tomasi C, Manduchi R. Bilateral filtering for gray and color images. IEEE International Conference on Computer Vision (ICCV) Bombay. 1998. p. 7.
[29] He KM, Sun J, Tang XO. Guided image filtering. European conference on computer vision (ECCV) Berlin. 2010.
[30] Jain P, Tyagi V. A survey of edge-preserving image denoising methods. Inf Syst Front 2016;18:159–70.
[31] Zhu KP, Mei T, Ye DS. Online condition monitoring in micromilling: a force waveform shape analysis approach. IEEE Trans Ind Electronics 2015;62:3806–13.
[32] a J, Castejóna M, Alegrea E, Hernándezb LK. Use of descriptors based on moments from digital images for tool wear monitoring. Int J Mach Tools Manuf 2008;48:1005–13.
[33] Liu TI. A computer vision approach for drill wear measurements. J Mater Shap Technol 1990;8:11–6.
[34] Malekian M, Park SS, Jun MBG. Tool wear monitoring of micro-milling operations. J Mater Process Technol 2009;209:4903–14.
[35] Fleischer J, Deuchert M, Ruhs C, Kühlewein C, Halvadjiysky G, Schmidt C. Design and manufacturing of micro milling tools. Microsyst Technol 2008;14:1771–5.
[36] Su JC, Huang CK, Tarng YS. An automated flank wear measurement of microdrills using machine vision. J Mater Process Technol 2006;180:328–35.
[37] Lee KH, Dornfeld DA. Micro-burr formation and minimization through process control. Precis Eng 2005;29:246–52.
[38] Attanasio A. Tool run-Out measurement in micro milling. Micromachines 2017;8(7):221.
[39] Castro HFF. A method for evaluating spindle rotation errors of machine tools using a laser interferometer. Measurement 2008;41(5):526–37.
[40] Li KX, Zhu KP, Mei T. A generic instantaneous undeformed chip thickness model for the cutting force modeling in micromilling. Int J Mach Tools Manuf 2016;105:23–31.